Middle to Late Pleistocene vegetation and climate change in subtropical southern East Africa

Isla S. Castañeda[1,2,*], Thibaut Caley[3,4], Lydie Dupont[5], Jung-Hyun Kim[1,6], Bruno Malaizé[3], and Stefan Schouten[1]

[1]*NIOZ Royal Netherlands Institute for Sea Research, Department of Marine Microbiology and Biogeochemistry, and Utrecht University, PO Box 59, 1790 AB Den Burg, The Netherlands*
[2]*University of Massachusetts Amherst, Department of Geosciences, 611 N Pleasant St., 233 Morrill Science Center II, Amherst, MA 01003 USA*
[3]*EPOC, UMR CNRS 5805, Université de Bordeaux, Allée Geoffroy St Hilaire, 33615 Pessac, France*
[4]*IFREMER, Laboratoire Environnements Sédimentaires, BP70, 29280 Plouzané, France*
[5]*MARUM Center for Marine Environmental Sciences, University of Bremen, Germany*
[6]*Department of Marine Science and Convergence Technology, Hanyang University ERICA Campus, 55 Hanyangdaehak-ro, Sangnok-gu, Ansan-si, Gyeonggi-do 426-791, South Korea*
**Corresponding author email: isla@geo.umass.edu*

Abstract:

In this study we investigate Pleistocene vegetation and climate change in southern East Africa by examining plant leaf waxes in a marine sediment core that receives terrestrial runoff from the Limpopo River. The plant leaf wax records are compared to a multi-proxy sea surface temperature (SST) record and pollen assemblage data from the same site. We find that Indian Ocean SST variability, driven by high-latitude obliquity, exerted a strong control on the vegetation of southern East Africa during the past 800,000 years. Interglacial periods were characterized by relatively wetter and warmer conditions, increased contributions of C_3 vegetation, and higher SST, whereas glacial periods were marked by cooler and arid conditions, increased contributions of C_4 vegetation, and lower SST. We find that Marine Isotope Stages (MIS) 5e, 11c, 15e and 7a-7c are strongly expressed in the plant leaf wax records but MIS 7e is absent while MIS 9 is rather weak. Our plant leaf wax records also record the climate transition associated with the Mid-Brunhes Event (MBE) suggesting that the pre-MBE interval (430-800 ka) was characterized by higher inputs from grasses in comparison to relatively higher inputs from trees in the post-MBE interval (430 to 0 ka). Differences in vegetation

and SST of southern East Africa between the pre- and post-MBE intervals appear to be related to shifts in the location of the Subtropical Front. Comparison with vegetation records from tropical East Africa indicates that the vegetation of southern East Africa, while exhibiting glacial-interglacial variability and notable differences between the pre- and post-MBE portions of the record, likely did not experience such dramatic extremes as occurred to the north at Lake Malawi.

1. Introduction

The Earth experienced numerous fluctuations between cold glacial periods and warm interglacial periods during the Pleistocene. Individual glacial and interglacial periods were characterized by varying boundary conditions including insolation, continental ice sheet extent and atmospheric carbon dioxide (pCO_2) concentrations, resulting in differing intensities and associated patterns of climate variability (Past Interglacials Working Group of PAGES, 2016). Accompanying glacial-interglacial variability, long-term climate transitions also occurred. During the mid-Pleistocene transition (1.2-0.6 Ma), variations in global ice volume shifted from exhibiting a dominant 41 kyr periodicity to a 100 kyr periodicity and a number of atmospheric and oceanic circulation changes took place (Past Interglacials Working Group of PAGES, 2016). Another climate transition, the Mid-Brunhes Event (MBE), placed between Marine Isotope Stages (MIS) 12/11 at 430 ka, marks an increase in the amplitude of glacial-interglacial cycles after this time (Jansen et al., 1986; EPICA community members, 2004).

On the African continent dramatic and rapid climate fluctuations frequently occurred during the Pleistocene, which are thought to have contributed to major steps in human evolution and to the development of modern behavior (e.g. Compton, 2011; deMenocal, 2004; Trauth et al., 2009). Presently, continuous records of African continental climate spanning beyond the Last Glacial

Maximum (MIS 2) are relatively rare. A number of Plio-Pleistocene marine records exist from the tropical and subtropical regions offshore northwest and northeast Africa (deMenocal, 2004) while numerous lakes and paleolakes of the East African Rift valley have provided both long, continuous records and brief snapshots into past climate during discrete intervals (e.g. Scholz et al., 2007; Cohen et al., 2007). These records reveal dramatic past hydroclimate and vegetation fluctuations as well as a high degree of spatial variability. In contrast, the subtropical southern African continent, a region that hosted early hominin species (e.g. Compton, 2011), remains understudied.

Here we examine plant leaf waxes from a marine sediment core to investigate vegetation change in southern East Africa during the past 800,000 years. We compare our records to pollen (Dupont et al., 2011) and sea surface temperature (SST) (Caley et al., 2011) reconstructions from the same core. Pollen and plant macrofossils are commonly used to examine vegetation change, a sensitive indicator of past climate conditions. A complementary approach is to examine the distribution and isotopic composition of plant leaf waxes. High molecular weight *n*-alkanes (29 to 33 carbon atoms) are a main component of plant epicuticular waxes (Eglinton and Hamilton, 1967). The distribution of dominant homologues can reflect environmental conditions while the carbon isotopic composition ($\delta^{13}C$) of *n*-alkanes provides information on the dominant photosynthetic pathway (C_3 or C_4) used (Collister et al., 1994). Our records provide insights into the role of Indian Ocean SST and orbital forcing in driving subtropical vegetation change.

2. Study location and methods

2.1 Study location

Giant piston core MD96-2048 (37.59m, 660m depth), located in the precursor region of the Agulhas Current, was retrieved by the R/V Marion Dufresne during the 104 MOZAPHARE cruise from

78 the upper continental slope offshore Mozambique, south of the Limpopo River mouth (26°10'S,
79 34°01'E) (Figure 1). The uppermost 12m of the core, spanning the past 800 ka, is examined. The age
80 model was previously published by Caley et al. (2011) and is based on oxygen isotope stratigraphy.
81 Pollen and spore analysis of the upper part of the core (MIS 9 to 1) is reported by Dupont et al.
82 (2011). The SST record is based on a stacked record of the $U_{37}^{K'}$ Index, the TEX_{86} paleothermometer
83 and Mg/Ca ratios of *G. ruber s.s.* (Caley et al., 2011).
84 The Limpopo River is the second largest African river draining into the Indian Ocean after the
85 Zambezi River. Its watershed includes parts of Botswana, Zimbabwe, southern Mozambique and
86 northern South Africa (Figure 1). Watershed elevation varies greatly ranging from lowland coastal
87 regions to >2000m on the interior central southern Africa plateau. Mean annual temperature and
88 precipitation ranges from 16°C and 1400mm in the central plateau region to 24°C and 600mm in the
89 lowlands (Dupont et al., 2011). Presently, a strong relationship exists between southwest (SW) Indian
90 Ocean SST and southern East African precipitation. Most rainfall occurs in austral summer (November
91 to March) with precipitation increasing in late summer when SW Indian Ocean SSTs are the highest
92 (Jury et al., 1993; Reason and Mulenga, 1999). The vegetation of the Limpopo catchment is highly
93 variable and includes closed forest, dry scrubland, alpine open grasslands and semi-evergreen
94 lowland forest (Figure 1; White, 1983). For a detailed description of modern vegetation in the
95 Limpopo catchment the reader is referred to Dupont et al. (2011).
96
97 ***2.2 Organic geochemical analyses***
98 177 samples from core MD96-2048 were freeze dried and extracted with an Accelerated
99 Solvent Extractor (ASE 200) using a mixture of 9:1 dichloromethane (DCM) to methanol (MeOH).
100 Samples were separated into apolar, ketone and polar fractions with alumina oxide using solvent

mixtures of 9:1 (vol:vol) hexane/DCM, 1:1 (vol:vol) hexane/DCM, and 1:1 (vol:vol) DCM/MeOH, respectively. The apolar fractions were passed through Ag^+ impregnated silica to separate saturated and unsaturated hydrocarbons.

Identification of *n*-alkanes was performed on a Thermo Finnigan Trace Gas Chromatograph (GC) Ultra coupled to Thermo Finnigan DSQ mass spectrometer (MS) using a CP Sil-5 fused silica capillary column (25m × 0.32mm; film thickness 0.12µm) with helium as the carrier gas. Mass scans were made from m/z=50–800 with 3 scans per second and an ionization energy of 70eV. The oven program initiated at 70°C, increased by a rate of 20°C min^{-1} to 130°C, and subsequently by a rate of 4°C min^{-1} until 320°C (held for 10 min).

Quantification of *n*-alkanes was performed on an HP 6890 gas chromatograph (GC) using a 50m CP Sil-5 column (0.32mm diameter, film thickness 0.12µm), helium as the carrier gas, and the same oven program as for GC-MS. Compound concentrations were determined by relating chromatogram peak areas to the concentration of an internal standard of known concentration. The average chain length (ACL; Poynter et al., 1989) was calculated using the C_{27} to C_{33} *n*-alkanes (many samples did not contain shorter homologues):

$$ACL = \frac{27C_{27}+29C_{29}+31C_{31}+33C_{33}}{(C_{27}+C_{29}+C_{31}+C_{33})},$$

where C_x represents the abundance of the *n*-alkane with *x* carbon atoms.

Compound-specific $\delta^{13}C$ analyses were performed on the aliphatic fraction using an Agilent 6800 GC coupled to a ThermoFisher Delta V isotope ratio monitoring mass spectrometer. Isotope values were measured against a calibrated external reference gas and instrument performance was monitored by daily injection of a mixture of C_{20} and C_{24} perdeuterated *n*-alkanes with known isotopic

compositions. Squalane added as an internal standard to each sample provided an additional check on instrument performance. The $\delta^{13}C$ values for individual compounds are reported in the standard delta notation against the Vienna Pee Dee Belemnite (VPDB) standard. Ninety nine samples were analyzed in duplicate to quadruplicate with a reproducibility of on average ±0.36‰ for the C_{31} *n*-alkane.

3. Results

Concentrations of total long-chain *n*-alkanes (C_{27}-C_{33}) vary from 0.02 to 0.82µg g sed^{-1} with a mean value of 0.27µg g sed^{-1}. In general, concentrations and mass accumulation rates (MAR) of *n*-alkanes do not exhibit clear glacial-interglacial patterns with a few exceptions (Figure 2). The lowest *n*-alkane concentrations and MARs are noted from ~491 to 522 ka during MIS 13. Elevated *n*-alkanes concentrations and MARs are noted during the MIS 2 and also in the older part of the core (526-620 ka and 680-800 ka). ACL ranges from 30.7 to 31.4 with a mean value of 30.9. Mean pre- and post-MBE (see section 4.5) ACL values are 31.0 and 30.9, respectively (Figure 2).

The C_{29}-C_{33} *n*-alkanes were generally present in suitable concentrations to analyze their carbon isotopic composition. Here we report the carbon isotope composition of the C_{31} *n*-alkane (hereafter $\delta^{13}C_{wax}$, n=166), the most abundant homologue. The C_{33} *n*-alkane was also abundant but it co-eluted with another compound so its isotopic composition could not be reliably measured. In core MD96-2048, $\delta^{13}C_{wax}$ values range from -23.8 to -27.9‰ (Figure 2), with a mean value of -25.5‰. The $\delta^{13}C_{wax}$ record indicates generally lower values during interglacials and higher values during glacials. The average $\delta^{13}C_{wax}$ values in the pre-MBE and post-MBE intervals are similar at -25.6‰ and -25.4‰, respectively. The uppermost sample analyzed from MD96-2048 (0.36 ka) has a $\delta^{13}C_{wax}$ value of -

25.8‰, similar to core top samples collected from 23-28°S from the Atlantic Ocean offshore western Namibia and South Africa, which vary from -25.2‰ to -26.1‰ (Vogts et al., 2012).

4. Discussion

4.1. Sources of n-alkanes

Plant leaf waxes are widely recognized as a resistant compound class and are known to be transported long-distances within large river systems (e.g. Ponton et al., 2014). Many previous studies have examined marine sediment cores situated in front of large river basins including the Nile (e.g. Castañeda et al., 2016), the Congo (e.g. Schefuß et al., 2003) and the Zambezi (e.g. Schefuß et al., 2011) to investigate basin-scale continental vegetation or hydroclimate change from leaf waxes, the approach we take here. A study of leaf wax hydrogen isotopes in Amazon River particulate organic matter, designed to test whether biomarkers present in rivers are representative of their catchment, concluded that leaf waxes in transit largely reflect catchment-averaged precipitation, thereby supporting this approach to paleoclimate reconstruction (Ponton et al., 2014).

Before inferring the vegetation and climatic history based on plant leaf waxes or pollen, the source area(s) of the vegetation must be determined. Plant leaf waxes are transported to marine sediments via wind or water erosion. Here, transport by the Limpopo River is likely the main transport mechanism as the dominant wind patterns do not facilitate transport of *n*-alkanes from the continent to the SW Indian Ocean because the surface airflow persists in an east-west (ocean to land) direction during most of the year (Tyson and Preston-Whyte, 2000). The coring site is also located close (within 120km) to the mouth of the Limpopo River (Figure 1). Furthermore, we note a significant positive correlation (r^2=0.78, $p<0.001$) between mass accumulation rates (MAR) of total *n*-alkanes and total branched glycerol dialkyl glycerol tetraethers (brGDGTs) (Figure 2). BrGDGTs are

169 commonly found in soils (Weijers et al., 2007) and their presence at site MD96-2048 is attributed to
170 Limpopo River runoff (Caley et al., 2011). Although overall terrestrial inputs to the coring site are low,
171 as evidenced by low concentrations of *n*-alkanes, brGDGTs (Caley et al., 2011), and pollen grains
172 (Dupont et al., 2011), the general agreement between brGDGT and *n*-alkane MARs (Figure 2)
173 suggests that fluvial transport is the dominant delivery mechanism of leaf waxes to site MD96-2048.
174 Dupont et al. (2011) also concluded that most of the pollen and spores at this site are fluvially
175 transported.

176 Based on pollen, Dupont et al. (2011) suggested that the main source area of material to
177 MD96-2048 is from the region north of Maputo, extending from the Drakensberg (the eastern
178 portion of the Great Escarpment) in the west to the coastal plain in the east (Figure 1). We assume
179 that plant leaf waxes in the same sediment core derive from an identical region. It should be noted
180 that the source area of material within the Limpopo River catchment may have shifted in the past
181 between different sub-basins under different climate regimes, as has been documented for other
182 large river catchments including the nearby Zambezi (Just et al., 2014; van der Lubbe et al., 2016).
183 However, this issue cannot be assessed for MD96-2048 with the data presently available. We note
184 that the Zambezi River likely does not represent a significant source of material to site MD96-2048.
185 Marine cores collected in front of the Zambezi and Limpopo Rivers reveal qualitative differences
186 between pollen assemblages, with pollen from the Limpopo site consistent with vegetation reflecting
187 overall lower temperatures (Dupont et al., 2011 and references therein) as expected for the more
188 southerly position of the Limpopo catchment. Furthermore, the core site is located in the southern
189 Limpopo cone deposition center, which has accumulated sediments since the Late Miocene, its
190 location restricted aerially by a counter-current (Martin, 1981). Sediment transport from the Zambezi
191 River is northwards over the shelf to the upper part of the deep sea canyon during interglacials

192 whereas sediment is mainly discharged on the slope in front of the river mouth during sea level
193 lowstands (Schulz et al. 2011; van der Lubbe et al. 2014). Therefore, it seems unlikely that Zambezi-
194 derived material deposited at these locations could be displaced to the Limpopo cone (upper slope),
195 over five degrees of latitude to the south.
196
197 ***4.2. Glacial-interglacial variability in plant leaf wax ratios***
198 Several parameters based on the distribution of *n*-alkane homologues reflect environmental
199 variability. For example, increasing ACL is observed with increasing aridity or temperature (e.g.
200 Poynter et al., 1989; Rommerskirchen et al., 2003; Horikawa et al., 2010; Bush and McInerney, 2015).
201 Likewise, the ratio of $C_{31}/(C_{29}+C_{31})$ *n*-alkanes, is also used as a proxy for temperature or aridity
202 (Horikawa et al., 2010). We focus leaf wax discussion on the $C_{31}/(C_{29}+C_{31})$ ratio, which most clearly
203 resolves the glacial/interglacial cycles. This ratio likely reflects vegetation change on the African
204 landscape as rainforest species dominantly produce the C_{29} *n*-alkane while savanna species
205 (including trees, herbs and shrubs) dominantly produce the C_{31} *n*-alkane (Vogts et al., 2009).
206 The glacial-interglacial cycles of the past 800 ka are strongly expressed in the $C_{31}/(C_{29}+C_{31})$
207 ratio except for Termination III, marking the transition between MIS 8/7, which is not expressed in
208 the *n*-alkane records (Figure 3). While the interval of substages 7a through 7c is marked by a clear
209 excursion to lower $C_{31}/(C_{29}+C_{31})$ values, the absence of substage 7e, coupled with a weak MIS 8
210 glacial, results in the absence of Termination III. In agreement with our data, MIS 7 is recognized as a
211 weak interglacial while the part of MIS 8 immediately before Termination III is a weak glacial at many
212 sites (Lang and Wolff, 2011). MIS 7 is a particularly intriguing interglacial as substage 7e is the
213 strongest signal at some locations whereas at others 7c is the strongest (Lang and Wolff, 2011). In
214 other records, the entire interval of 7c through 7a appears as a rather strong interglacial (Lang and

Wolff, 2011), which is the case for our vegetation records. Of the interglacials, MIS 11 and MIS 5 are recognized as the strongest of the past 800 ka with MIS 11 being exceptionally strong (Lang and Wolff, 2011). Both MIS 5e and 11c are clearly expressed in our leaf wax records, as is MIS 15e. Termination II, marking the transition from MIS 6/5, is particularly dramatic and abrupt in the $C_{31}/(C_{29}+C_{31})$ record (Fig. 3). Interestingly, while MIS 9 is recognized as a strong interglacial at many sites, including in the MD96-2048 SST record, it is relatively weak in the $C_{31}/(C_{29}+C_{31})$ record. Conversely, we also note that SW Indian Ocean SST was quite low during MIS 7a-c when a relatively strong response in the $C_{31}/(C_{29}+C_{31})$ record is detected. While the reasons for a weak expression of MIS 9 and a strong expression of 7a-c in our *n*-alkane records are not clear, likely other factors in addition to aridity, which in turn is related to SST variability, contributed to vegetation change at these times. Overall, the $C_{31}/(C_{29}+C_{31})$ record supports stronger glacial-interglacial vegetation variability in southern East Africa since the MBE (EPICA community members 2004; Lang and Wolff, 2011).

Interestingly, a long term trend to lower ACL and $C_{31}/(C_{29}+C_{31})$ ratios occurs from 800 ka to the present. A long-term trend to lower SST also occurs over this interval (Figure 3). While the SST trend is largely due to pronounced cooling during MIS 2, at ODP Site 1082, located offshore Namibia at 21.5°S, the opposite trend is observed where a long-term shift to lower oxygen isotope values of *Globorotalia inflata* reflects increasingly higher glacial SSTs toward the present (Jahn et al., 2003). This pattern may be related to long-term variability in the location of the Subtropical Front (STF), and the associated strength and position of the Agulhas Current and Agulhas Leakage (see section 4.5). However, the exact cause of the long term decrease in the $C_{31}/(C_{29}+C_{31})$ ratio remains unclear.

4.3 Leaf wax proxies and pollen

238 The stable carbon isotopic composition of plant leaf waxes ($\delta^{13}C_{wax}$) is used to distinguish
239 vegetation utilizing the two major photosynthetic pathways. The C_3 pathway is the most common
240 and is used by most trees, cold-season grasses and sedges while the C_4 pathway is utilized by warm
241 season grasses and sedges and is common in tropical savannas. C_3 plants have lower carbon isotopic
242 values in comparison to C_4 vegetation (Collister et al., 1994). For the C_{31} *n*-alkane, mean values of -
243 35.2‰ and -21.7‰ are representative of C_3 and C_4 vegetation, respectively (Castañeda et al., 2009a).
244 A third photosynthetic carbon-fixation pathway, the Crassulacean Acid Metabolism pathway, is
245 typically used by a minor component of the vegetation and has isotopic values intermediate
246 between those of C_3 and C_4 plants (Feakins and Sessions, 2010). Recent work indicates a larger
247 variability in the range of C_3 plant carbon isotope values than previously thought (Diefendorf et al.,
248 2010). However, C_3 vegetation is generally isotopically depleted in ^{13}C comparison to C_4 vegetation
249 and thus $\delta^{13}C_{wax}$ can be used to examine relative inputs of C_3 vs. C_4 plants, although absolute values
250 should be interpreted with care. A number of factors including temperature, aridity and pCO_2 can
251 influence the distribution of C_3 and C_4 vegetation (e.g. Kohn et al., 2014 and references therein). In
252 tropical Africa previous studies have recognized aridity (precipitation) as the main factor controlling
253 the continental scale distribution of C_3 vs. C_4 vegetation (e.g. Castañeda et al., 2009a; Schefuß et al.,
254 2003) although more recent work suggests a greater influence of temperature and CO_2, particularly
255 for glacial periods (Kohn et al., 2014).
256 We find that ACL, the $C_{31}/(C_{29}+C_{31})$ ratio, and $\delta^{13}C_{wax}$ of MD96-2048 reveal similar overall
257 trends (Figure 3). Glacial periods are generally characterized by higher ACL values, higher
258 $C_{31}/(C_{29}+C_{31})$ ratios and higher $\delta^{13}C_{wax}$ values. A study of the central USA found longer *n*-alkane chain
259 lengths, and higher ACL values, were correlated with higher growing season temperature (Bush and
260 McInerney, 2015). Likewise, to the north of the Limpopo basin at Lake Malawi, higher ACL values also

261 are correlated with higher temperatures (Castañeda et al., 2009b). Conversely, in core MD96-2048
262 higher ACL values are noted during glacials, suggesting that temperature likely is not the dominant
263 controlling factor on *n*-alkane chain length. Increased *n*-alkane chain lengths are also associated with
264 increased aridity (Poynter et al., 1989; Schefuß et al., 2003). Thus in the Limpopo River drainage
265 aridity or relative humidity is likely the main control on *n*-alkane chain length. The $\delta^{13}C_{wax}$ record
266 indicates that glacial periods were also characterized by slightly higher contributions of C_4 vegetation
267 (Figure 3) although pollen data from the same core (Dupont et al., 2011) indicates that glacial-
268 interglacial changes in the extent of grassy vegetation were not large. Dupont et al. (2011) infer that
269 the combination of moderately less rainfall with lower temperatures drove the expansion of
270 mountain vegetation during glacial periods.

271 To date a relatively limited number of studies have examined pollen and $\delta^{13}C_{wax}$ from the
272 same samples (e.g. Huang et al., 2006; Rommerskirchen et al., 2006; Feakins et al., 2013; Hoetzel et
273 al., 2013; Dupont et al., 2013). Plant leaf waxes provide complementary, but different, information on
274 past vegetation assemblages in comparison to pollen. A fundamental difference is that *n*-alkanes are
275 an indicator of biomass whereas pollen is a signal of reproduction (e.g. Hughen et al., 2004). Pollen
276 can differentiate vegetation at the genus to species level whereas leaf wax distributions can provide
277 insight into general plant life forms (e.g. trees or grasses). Another difference is that pollen grains
278 from C_3 and C_4 grasses are microscopically indistinguishable (Bonnefille and Riollet, 1980) whereas
279 $\delta^{13}C_{wax}$ can differentiate vegetation using C_3 and C_4 photosynthesis. Some plant species produce little
280 pollen while others produce abundant pollen. Likewise, different species of plants produce variable
281 concentrations of leaf waxes (e.g. Vogts et al., 2009), which potentially could lead to a bias in $\delta^{13}C_{wax}$
282 if large differences in *n*-alkane concentrations exist between C_3 and C_4 species. Both pollen and leaf

283 waxes may be transported by wind and fluvial erosion; however, some pollen types may be
284 selectively dispersed by animal vectors while other types are transported long distances by wind.

285 During the past 800 ka, our *n*-alkane records suggest interglacial periods in southern East
286 Africa were characterized by relatively wetter conditions with slightly increased contributions of C_3
287 vegetation. In contrast, glacial periods were characterized by more arid conditions and relatively
288 higher contributions of C_4 vegetation (Figures 3, 4). Overall, our *n*-alkane records support the pollen
289 data from the same core, covering the interval from 342 ka to the present (Dupont et al., 2011).
290 MD96-2048 pollen and spore counts were examined by applying a multivariate analysis in the form
291 of an endmember model unmixing procedure to generate a model consisting of three endmembers
292 (EM) (Figure 4; Dupont et al., 2011). EM1 represents humid mountainous *Podocarpus* forest and
293 woodland taxa, EM2 represents mainly open mountain vegetation dominated by ericaceous scrubs
294 (Ericaceae and Asteroideae) with a swampy component (including Cyperaceae, *Stipularia africana* and
295 *Typha*), and EM3 represents a complex situation of different biomes with woodland and forest taxa
296 combined with coastal vegetation (Dupont et al., 2011). EM1 is the most abundant during periods of
297 intermediate climate between full interglacial and full glacial conditions (MIS 9, 7 and the later part
298 of MIS 5), EM2 is most abundant during full glacial periods (MIS 8, 6 and 2-4) while EM3 is most
299 abundant during full interglacial stages (MIS 9, 7, 5e and 1) (Figure 4). Dupont et al. (2011) found that
300 the extent of EM2 (open mountain vegetation) in southern East Africa was driven primarily by SST in
301 this region of the SW Indian Ocean. Here, we also note agreement between the *n*-alkane and SST
302 records (see section 4.4).

303 To investigate relationships between pollen assemblages and *n*-alkane parameters ($\delta^{13}C_{wax}$ and
304 the $C_{31}/(C_{29}+C_{31})$ ratio), correlations were performed with each of the three endmembers. The
305 $C_{31}/(C_{29}+C_{31})$ ratio was found to exhibit a significant correlation with EM2 ($r=0.63$, $p<0.001$) but not

306 with EM1 or EM3. Similarly, the $\delta^{13}C_{wax}$ record, although of lower sampling resolution, also reveals a
307 significant correlation with EM2 ($r=0.47$, $p<0.001$). General trends in both records track overall
308 changes in EM2 (Figure 4); thus it appears that the *n*-alkanes are sensitive to variability in open
309 mountain vegetation. This finding is in agreement with a study of *n*-alkane distributions in modern
310 African vegetation, which found that found savanna herbs, trees and shrubs (i.e. shrubby open
311 mountain vegetation) are dominated by the C_{31} *n*-alkane whereas rain forest vegetation is
312 dominated by the C_{29} *n*-alkane (Vogts et al., 2009).

313 Although our $\delta^{13}C_{wax}$ record shows similar overall patterns to the $C_{31}/(C_{29}+C_{31})$ ratio, it is
314 relatively more noisy because the analytical error (0.3-0.5‰) is more significant relative to the range
315 (Figures 3, 4). The maximum overall range of the Limpopo River $\delta^{13}C_{wax}$ record is 4.1‰ but generally
316 glacial-interglacial changes are around 2.5‰. Such glacial-interglacial shifts in $\delta^{13}C_{wax}$ are relatively
317 small in comparison to other East African sites. At Lake Tanganyika (Tierney et al., 2010) and Lake
318 Challa (Sinninghe Damsté et al., 2011), $\delta^{13}C_{wax}$ values vary by approximately 10‰ and 9‰,
319 respectively, between the LGM and the early Holocene. In contrast, a marine core from offshore
320 south western Africa (23°S) exhibits glacial-interglacial shifts in $\delta^{13}C_{wax}$ of ~2.5‰ (Collins et al., 2014).
321 The relatively small range in $\delta^{13}C_{wax}$ is likely because the Limpopo drainage, and also western
322 southern Africa (Collins et al., 2014), did not experience major C_3/C_4 interglacial-glacial shifts like
323 tropical East Africa experienced. The open mountain vegetation assemblage of EM2 includes the
324 families Cyperaceae, Asteraceae, and Poaceae, which contain some C_4 species (Dupont et al., 2011).
325 However, the abundance of Cyperaceae and Asteraceae pollen is low and is likely related to coastal
326 vegetation while Poaceae (includes C_3 and C_4 species) scores only 14% of the taxa on the EM2
327 assemblage (Dupont et al., 2011). EM3, representing a vegetation complex similar to the present with
328 grasslands present on the interior plateau and forest in the lowlands, also contains Poaceae, which

scores about 20% on EM3 (Dupont et al., 2011). Due to the opposing pattern of EM2 dominating during full glacials and EM3 dominating during full interglacials, and the fact that C_4 vegetation is not a dominant component of either end member, it appears that southern East Africa did not experience major glacial/interglacial shifts in C_3 vs. C_4 plant dominance. This may explain why the $\delta^{13}C_{wax}$ record lacks well-defined glacial/interglacial cycles that are better resolved by the $C_{31}/(C_{29}+C_{31})$ ratio.

4.4 SST, orbital forcing and vegetation change in SE Africa

Currently, a strong relationship exists between western Indian Ocean SST and summer rainfall in northern South Africa (Jury et al., 1993; Reason and Mulenga, 1999). A main finding of the pollen analysis of MD96-2048 is that SW Indian Ocean SST was a main control on the extent of open mountain vegetation (EM2) during the past 350 ka (Dupont et al., 2011). We also note a significant negative correlation between the $C_{31}/(C_{29}+C_{31})$ ratio and the SST stack of MD96-2048 ($r=-0.69$, $p<0.001$), after detrending to remove the long-term trend to lower values, further supporting that SW Indian Ocean SST has been a main control on the vegetation of southern East Africa during the past 800 ka. The $\delta^{13}C_{wax}$ record exhibits a significant but weaker correlation with the SST stack ($r=-0.48$, $p<0.001$), likely due to the relatively larger noise.

It was previously found that SST and a qualitative salinity record of MD96-2048 contained strong 100 kyr and 41 kyr cycles (Caley et al., 2011). Likewise, it was found that pollen EM2 (open mountain vegetation) abundances displayed significant power at the 100 kyr and 41 kyr periodicities (Dupont et al., 2011), anti-phased with the SST record (e.g. higher proportions of EM2 coincide with lower SST; Figure 4). While the 100 kyr signal is present in the SST and vegetation records, Caley et al. (2011) found that eccentricity forcing is not significant at site MD96-2048 based on the observation

of weak 23 and 19 kyr precession signals, which are modulated by eccentricity, and concluded that high latitude obliquity is the main driver of the Agulhas current system. Spectral analysis of the $C_{31}/(C_{29}+C_{31})$ ratio also reveals strong 100 kyr and 41 kyr cycles (Figure 5), coherent at the 95% confidence level, further supporting the role of obliquity in driving vegetation change in southern East Africa (Dupont et al., 2011; Caley et al., 2011). We note that the amplitude of the precession signal may be dampened in the pollen and *n*-alkane records due to a sampling resolution with an average time step of 4.5 kyr. However, a Mg/Ca SST record from this core with a mean time step of 2.5 kyr also failed to yield a precession signal; thus precession likely does not drive SW Indian Ocean SST variability (Caley et al., 2011). Dupont et al. (2011) note that the coring site is at the southern limit of the subtropics and receives seasonal rainfall characteristic of monsoonal climates but not a seasonal wind reversal so a strong influence of precession is not expected in contrast to more equatorial sites. Spectral analysis was conducted on all *n*-alkane parameters but none were found to exhibit a significant precession signal.

4.5 The MBE in southern East Africa

The Mid-Brunhes Event (MBE) is a climate transition that occurred between Marine Isotope Stages (MIS) 12/11 (Jansen et al., 1986; EPICA community members, 2004). Antarctic and Southern Ocean records reveal that prior to the MBE interglacials were characterized by higher global ice volume, lower pCO_2 and lower temperatures in comparison to post-MBE interglacials (EPICA community members, 2004; Jouzel et al., 2007, Yin, 2013). The MBE is reported in numerous paleoclimate archives, especially from the southern hemisphere. It is debated whether the MBE was a global or regional event as some records, particularly terrestrial records, do not capture the MBE (e.g. Candy et al., 2013; Meckler et al., 2012). The vegetation records of MD96-2048 provide insight into

375 the MBE from a subtropical continental setting. In the subsequent discussion we examine two
376 intervals: 800-430 ka (pre-MBE) and 430-0 ka (post-MBE) (Yin, 2013; EPICA community members,
377 2004).

378 Most *n*-alkane parameters exhibited statistically significant differences at the 95% confidence
379 level between the pre- and post-MBE intervals as determined from a two sample Student's t-test,
380 after first performing an F-test to determine equality of variances. Based on the outcome of the F-
381 test for each *n*-alkane parameter, the appropriate t-test (either assuming unequal or equal variances)
382 was conducted. Only the $\delta^{13}C_{wax}$ record did not show a significant difference between pre- and post-
383 MBE values ($p>0.05$). We find that the pre-MBE interval is characterized by higher mean ACL and
384 $C_{31}/(C_{29}+C_{31})$ values (Figure 6). In the EPICA Dome C deuterium isotope (δD) record (not plotted), the
385 MBE transition is not expressed by a change in the mean value of the pre- and post-MBE intervals
386 but rather the post-MBE interval is characterized by a larger amplitude in δD values (EPICA
387 community members, 2004). In the EPICA Dome C pCO_2 (Lüthi et al., 2008) and global benthic
388 oxygen isotope (Lisiecki and Raymo, 2005) records, a change in both the mean and amplitude is
389 noted between the pre-and post-MBE intervals (Figure 6). Most of our records, including the SST
390 stack, also indicate a change in amplitude between the pre- and post-MBE intervals (Figure 6). We
391 note that we have not excluded MIS 7, recognized as a weak interglacial, or MIS 19, recognized as a
392 strong interglacial, in our analysis as Yin (2013) did, although doing so would result in even more
393 pronounced pre- and post-MBE differences. Overall, our *n*-alkane records indicate that increased
394 shrubby vegetation characterized the pre-MBE interval.

395 Shifts in the location of oceanic fronts were likely a main cause of differences in the
396 vegetation and climate of southern East Africa on glacial-interglacial timescales as well as in the pre-
397 versus post-MBE intervals. On glacial-interglacial timescales, proxy data indicate that in the SW

Indian Ocean, the STF shifted northwards during glacials and southwards during interglacials of the past 1.5 Ma (Bard and Rickaby 2009; Caley et al., 2011; Caley et al., 2012). The relative position of the STF exerts an influence on SW Indian Ocean SST in addition to temperature changes associated with insolation-driven glacial-interglacial cycles. Within this context, it is recognized that when the STF reached its most northerly position, such as during MIS 10 and 12, glacial SSTs at MD96-2048 were relatively mild (Caley et al., 2011). In the SW Indian Ocean, an opposite SST response occurs between sites MD96-2048 (26°S) and MD96-2077 (33°S) (Bard and Rickaby, 2009). At site MD96-2077, located near to the present day position of the STF (Figure 1), extreme northward migration of the STF results in lower SST whereas site MD96-2048 experiences higher SST. This pattern is expected from a northward migration of the STF, which is associated with a contraction of the subtropical gyre and causes the location of the Agulhas retroflection to be shifted to the north and restricted within the Indian Ocean (Sjip and England, 2008).

It appears that shifts in the location of the STF also caused differences in vegetation and SST between the pre- and post-MBE intervals. Our data suggests that in the post-MBE interval both interglacial and glacial periods were characterized by relatively larger inputs of trees and relatively lower SSTs in comparison to the pre-MBE interval. At the Angola Basin, Jansen et al. (1986) report a change from more arid to more humid conditions at 400-350 ka. Yin (2013) examined individual interglacial responses to variable insolation forcing and found that stronger westerlies characterized pre-MBE interglacials, which increased Southern Ocean upwelling and enhanced Antarctic Bottom Water formation. This caused the Antarctic Polar Front (Yin, 2013) and the STF to be located in relatively more northerly positions during the pre-MBE interglaicals (Q. Yin, personal communication, 2015). Relatively higher SST at site MD96-2048 during both glacials and interglacials of the pre-MBE interval support an overall more northerly position of the STF, corroborating the results of Yin (2013).

421 Interestingly, higher SSTs in the pre-MBE interval are seemingly at odds with the plant leaf
422 wax data suggesting overall increased inputs from grasses (C_{31}), which we interpret as mainly
423 reflecting aridity on glacial-interglacial timescales (see section 4.3). In the modern, higher Indian
424 Ocean SST is associated with increased rainfall in East Africa (Jury et al., 1993; Reason and Mulenga,
425 1999). However, as noted previously (section 4.2), especially strong glacials/interglacials in the alkane
426 records do not always coincide with strong expression in the SST record, implying a role for other
427 factors in driving vegetation change. A study by Kohn et al. (2014) combined paleoecological data
428 and model simulations to examine impacts of rainfall, pCO_2 and temperature on Holocene and LGM
429 (MIS 2) vegetation of the Zambezi River basin. Through different model experiments, they found that
430 precipitation and pCO_2 alone could not account for C_3/C_4 vegetation shifts in the Zambezi basin
431 inferred from $\delta^{13}C_{wax}$. Their study indicates that relatively small temperature changes are important
432 for driving C_3/C_4 shifts with Holocene vegetation controlled by precipitation and temperature, and
433 LGM vegetation mainly controlled by temperature and pCO_2 (Kohn et al., 2014). Furthermore, they
434 suggested that temperature influenced the vegetation of southern tropical Africa on long timescales
435 (Kohn et al., 2014). Lower pCO_2 and lower temperatures characterize pre-MBE interglacials (EPICA
436 community members, 2004; Jouzel et al., 2007, Yin, 2013). Thus, lower temperatures combined with
437 lower pCO_2 perhaps favored grasses (C_{31}) over trees (C_{29}) in the pre-MBE interval despite somewhat
438 higher SST locally.
439 The strength of the westerlies, and by association the position of the STF, also plays a crucial
440 role in the strength of the Agulhas Current system and leakage (e.g. Caley et al., 2012; Durgadoo et
441 al., 2013). Shifting the STF to the north results in reduced Agulhas leakage (Caley et al., 2012); thus,
442 the overall effect is that reduced Agulhas leakage characterized the pre-MBE interval. The Agulhas
443 leakage transfers heat and salt from the Indian Ocean to the Atlantic Ocean and affects variability in

444 the Atlantic Meridional Overturning Circulation (AMOC) (Caley et al., 2014; Peeters et al. 2004; Weijer
445 et al., 2002), which may explain why the MBE is noted in terrestrial records from Spain (Blain et al.,
446 2012). Increased Agulhas leakage during post-MBE glacials could also explain why the ODP Site 1082
447 (Figure 1) planktonic $\delta^{18}O$ record shows higher glacial SSTs in the post-MBE interval (Jahn et al.,
448 2003). Lower SSTs at site MD96-2048 in conjunction with higher SSTs at ODP Site 1082 are consistent
449 with increased Agulhas leakage during post-MBE glacials. Outside of the southern high latitudes and
450 locations that directly fall under the influence of the Antarctic Polar Front or the STF, regions that are
451 sensitive to AMOC variability may be well suited for recording the MBE.
452
453 ***4.6. Variability in mid- to late-Pleistocene African landscapes***
454 The African landscape is recognized as important to hominin development and therefore
455 understanding the mechanisms driving vegetation dynamics on a variety of timescales is of interest.
456 Pleistocene vegetation records reveal highly variable conditions across the African continent. A
457 compilation of West African marine pollen records indicates that despite strong fluctuations, the
458 latitudinal arrangement of biomes has been conserved through the past three or four climate cycles
459 (Dupont, 2011). There is some tendency toward increased forest vegetation during interglacials while
460 during glacials an equatorward savanna shift into the modern rain forest area is suggested (Dupont,
461 2011). At elevated areas open mountainous scrubland was widespread during the glacials,
462 alternating with phases in which mountain forests expanded, with *Podocarpus* maxima falling mostly
463 between the extremes of full glacials or full interglacials (Dupont 2011).
464 At Lake Malawi (11° S) multi-proxy records including pollen indicate a "megadrought",
465 occurring during MIS 6 and persisting for 18,000 years (Lane et al., 2013; Beuning et al., 2011; Scholz
466 et al., 2007; Cohen et al., 2007). During the megadrought, the volume of water in Lake Malawi was

467 reduced by at least 95% (Scholz et al., 2007) and grass-dominated vegetation was limited, implying
468 extreme aridity and suggesting conditions that would have been inhospitable to humans in the
469 region (Beuning et al., 2011). Our Limpopo basin vegetation records contrast significantly as we find
470 no evidence of the megadrought (Figure 4) suggesting that the extreme aridity was confined to more
471 tropical sites. In MD96-2048, the proportion of EM1, reflecting mainly humid mountainous
472 *Podocarpus* forest, is relatively high at this time (Dupont et al., 2011) while no significant changes in
473 the $C_{31}/(C_{29}+C_{31})$ ratio or $\delta^{13}C_{wax}$ are observed (Figure 4). Although glacial-interglacial changes in the
474 vegetation of southern East Africa are observed, notably woodland/forest pollen persists throughout
475 the entire record (Dupont et al., 2011) (Figure 4). The continued presence of trees on the landscape
476 indicates substantially less variability in the vegetation of southern East Africa in comparison to the
477 Lake Malawi region. Beuning et al. (2011) noted consistency between Lake Malawi and West African
478 pollen records (Angola and Congo basins) and suggested that large scale vegetation changes were
479 not controlled by SST but rather by changes in Hadley circulation or ITCZ position, which would be
480 sensitive to precession. However, we find that SW Indian Ocean SST variability, driven by obliquity,
481 exerted the main control on southern East African vegetation. Dupont (2011) concluded that while
482 the representation of tropical rain forest fluctuated with summer insolation and precession, the
483 subtropical biomes showed more obliquity variability or followed the pattern of glacial and
484 interglacials.

485 The emerging picture is that Pleistocene environments of the southern African continent
486 were more stable in contrast to those of tropical Africa. In recent years the southern African
487 continent has received an increasing amount of attention as a region critical to hominin evolution
488 and the appearance of modern behavior (Compton, 2011). Our results support the hypothesis that
489 the southern African continent provided suitable living environments for hominins and fauna

490 throughout the Pleistocene, which may have been especially important at times when tropical
491 Eastern Africa experienced extreme aridity.
492
493 **5. Conclusions**
494 Paired analyses of plant leaf waxes and pollen assemblages reveal insights into Pleistocene
495 vegetation change in southern East Africa. We find that while the Limpopo River basin did not
496 experience major glacial-interglacial changes in C_3 vs. C_4 vegetation, *n*-alkanes chain lengths are
497 sensitive to varying inputs of open mountain vegetation, which is closely tied to SW Indian Ocean
498 SST. In turn, the SST of the SW Indian Ocean largely reflects changes in high-latitude obliquity. Our
499 leaf wax records indicate a clear response of the southern East African vegetation to glacial-
500 interglacial climate variability as well as to the MBE. Differences between pre- and post-MBE
501 vegetation and climate of southern East Africa are attributed to shifts in the position of the STF, and
502 associated changes in the strength of the Agulhas leakage and AMOC may have been important for
503 transmitting the MBE outside of the southern high latitudes. Overall, our vegetation records indicate
504 that while glacial-interglacial changes in vegetation assemblages occurred, and a long-term shift
505 took place over the past 800 ka, in general landscapes of subtropical southern East Africa were
506 relatively stable compared to those of tropical East Africa. The relatively stable Pleistocene
507 environments of southern East Africa may have provided an important refuge for early hominins and
508 fauna at times when inhospitable conditions occurred in tropical East Africa.
509
510 **Acknowledgements**
511 We thank Michiel Kienhuis, Monique Verweij, Marianne Baas, Ellen Hopmans and Jort Ossebaar for
512 analytical assistance. Qiuzhen Yin is especially acknowledged for examining her model output from

513 Yin (2013) to investigate the movement of the subtropical front during pre- and post-MBE
514 interglacials. We are grateful to Dr. Jessica Tierney and an anonymous reviewer for insightful
515 comments that helped clarify and improve the manuscript. The Netherlands Organization for
516 Scientific Research (NWO) is thanked for financial support through a VICI grant to S. Schouten. Core
517 MD96-2048 was collected during the MOZAPHARE cruise of the RV Marion Dufresne, supported by
518 the French agencies Ministère de l'Education Nationale de la Recherche et de la Technologie, Centre
519 National de la Recherche Scientifique (CNRS), and Institut Paul Emile Victor (IPEV). This work was
520 supported by the "Laboratoire d'Excellence" LabexMER (ANR-10-LABX-19) and co-funded by a grant
521 from the French government under the program "Investissements d'Avenir", and by a grant from the
522 Regional Council of Brittany (SAD programme).

References

Bard, E., & Rickaby, R. E. Migration of the subtropical front as a modulator of glacial climate. *Nature*, 460, 380-383, 2009.

Beuning, K. R., K. A. Zimmerman, S. J. Ivory and A. S. Cohen, Vegetation response to glacial-interglacial climate variability near Lake Malawi in the southern African tropics, *Palaeogeography Palaeoclimatology Palaeoecology, 303*, 81-92, 2011.

Blain, H. A., G. Cuenca-Bescos, I. Lozano-Fernandez, J. M. Lopez-Garcia, A. Olle, J. Rosell and J. Rodriguez, Investigating the Mid-Brunhes Event in the Spanish terrestrial sequence, *Geology, 40*, 1051-1054, 2012.

Bonnefille, R. and G. Riollet, Pollen des savanes d'Afrique orientale: Éditions du Centre National de la Recherche Scientifique, Paris, 140 p., 113 plates, 1980.

Bush, R. T., & McInerney, F. A. Influence of temperature and C_4 abundance on *n*-alkane chain length distributions across the central USA. *Organic Geochemistry, 79*, 65-73, 2015.

Caley, T., J. H. Kim, B. Malaize, J. Giraudeau, T. Laepple, N. Caillon, K. Charlier, H. Rebaubier, L. Rossignol, I. Castañeda, S. Schouten and J.S. Sinninghe Damste, High-latitude obliquity as a dominant forcing in the Agulhas current system, *Climate of the Past, 7*, 1285-1296, 2011.

Caley, T., Giraudeau, J., Malaizé, B., Rossignol, L., & Pierre, C. Agulhas leakage as a key process in the modes of Quaternary climate changes. *Proceedings of the National Academy of Sciences*, *109*, 6835–6839, 2012.

Caley, T., Peeters, F. J., Biastoch, A., Rossignol, L., Sebille, E., Durgadoo, J., Malaizé, B., Giradeau, J., Arthur, K., Zahn, R. (2014). Quantitative estimate of the paleo-Agulhas leakage. *Geophysical Research Letters, 41*, 1238-1246.

545 Candy, I. and Mcclymont, E.L., 2013. Interglacial intensity in the North Atlantic over the last 800 000
546 years: investigating the complexity of the mid-Brunhes Event. *Journal of Quaternary Science, 28*, 343-348.
548 Castañeda, I.S., Schouten, S., Pätzold, J., Lucassen, F., Kasemann, S., Kuhlmann, H. and Schefuß, E.,
549 2016. Hydroclimate variability in the Nile River Basin during the past 28,000 years. *Earth and*
550 *Planetary Science Letters, 438*, 47-56.
551 Castañeda, I. S., S. Mulitza, E. Schefuss, R. A. L. dos Santos, J. S. Sinninghe Damsté and S. Schouten,
552 Wet phases in the Sahara/Sahel region and human migration patterns in North Africa, *Proc.*
553 *Natl. Acd. Sci. USA, 106*, 20159-20163, 2009a.
554 Castañeda, I. S., Werne, J. P., Johnson, T. C., & Filley, T. R. Late Quaternary vegetation history of
555 southeast Africa: the molecular isotopic record from Lake Malawi. *Palaeogeography,*
556 *Palaeoclimatology, Palaeoecology*, *275*, 100-112, 2009b.
557 Collins, J. A., Schefuß, E., Govin, A., Mulitza, S., and Tiedemann, R. Insolation and glacial–interglacial
558 control on southwestern African hydroclimate over the past 140 000 years. *Earth and*
559 *Planetary Science Letters*, *398*, 1-10, 2014.
560 Collister, J. W., G. Rieley, B. Stern, G. Eglinton and B. Fry, Compound-Specific Delta-C-13 Analyses of
561 Leaf Lipids from Plants with Differing Carbon-Dioxide Metabolisms, *Organic Geochemistry,*
562 *21*, 619-627, 1994.
563 Cohen, A.S., Stone, J.R., Beuning, K.R., Park, L.E., Reinthal, P.N., Dettman, D., Scholz, C.A., Johnson, T.C.,
564 King, J.W., Talbot, M.R. and Brown, E.T., 2007. Ecological consequences of early Late
565 Pleistocene megadroughts in tropical Africa. *Proceedings of the National Academy of*
566 *Sciences, 104,* 16422-16427.

567 Compton, J. S., Pleistocene sea-level fluctuations and human evolution on the southern coastal plain
568 of South Africa, *Quaternary Sci. Rev., 30*(5-6), 506-527, 2011.
569 deMenocal, P.B., 2004. African climate change and faunal evolution during the Pliocene–Pleistocene.
570 *Earth and Planetary Science Letters, 220*, 3-24.
571 Diefendorf, A. F., K. E. Mueller, S. L. Wing and K. H. Freeman, Global patterns in leaf ^{13}C discrimination
572 and implications for studies of past and future climate, *Proceedings of the National Academy*
573 *of Sciences, 107*, 5738-5743, 2010.
574 Dupont, L., Orbital scale vegetation change in Africa, *Quaternary Science Reviews, 30*, 3589-3602,
575 2011.
576 Dupont, L. M., Caley, T., Kim, J. H., Castañeda, I., Malaizé, B., & Giraudeau, J. Glacial-interglacial
577 vegetation dynamics in South Eastern Africa coupled to sea surface temperature variations in
578 the Western Indian Ocean. *Climate of the Past*, 7, 1209-1224, 2011.
579 Dupont, L. M., Rommerskirchen, F., Mollenhauer, G., & Schefuß, E. Miocene to Pliocene changes in
580 South African hydrology and vegetation in relation to the expansion of C_4 plants. *Earth and*
581 *Planetary Science Letters*, *375*, 408-417, 2013.
582 Durgadoo, J. V., Loveday, B. R., Reason, C. J., Penven, P., & Biastoch, A. Agulhas leakage
583 predominantly responds to the Southern Hemisphere westerlies. Journal of Physical
584 Oceanography, 43, 2113-2131, 2013.
585 Eglinton, G. and R. J. Hamilton, Leaf Epicuticular Waxes, *Science, 156*, 1322-&, 1967.
586 EPICA Community Members. Eight glacial cycles from an Antarctic ice core. *Nature*, 429, 623-628,
587 2004.
588 Feakins, S. J. and A. L. Sessions, Crassulacean acid metabolism influences D/H ratio of leaf wax in
589 succulent plants, *Org. Geochem., 41*, 1269-1276, 2010.

590 Feakins, S. J. Pollen-corrected leaf wax D/H reconstructions of northeast African hydrological changes
591 during the late Miocene.*Palaeogeography, Palaeoclimatology, Palaeoecology*, *374*, 62-71,
592 2013.
593 Hoetzel, S., Dupont, L., Schefuß, E., Rommerskirchen, F., & Wefer, G. The role of fire in Miocene to
594 Pliocene C_4 grassland and ecosystem evolution. *Nature Geoscience*, *6*, 1027-1030, 2013.
595 Horikawa, K., M. Murayama, M. Minagawa, Y. Kato and T. Sagawa, Latitudinal and downcore (0-750
596 ka) changes in *n*-alkane chain lengths in the eastern equatorial Pacific, *Quaternary Res., 73*,
597 573-582, 2010.
598 Huang, Y., B. Shuman, Y. Wang, T. Webb III, E. C. Grimm and J. Jacobson, Climatic and environmental
599 controls on the variation of C_3 and C_4 plant abundances in central Florida for the past 62,000
600 years, *Palaeogeogr. Palaeoclimatol. Palaeoecol., 237*, 428-435, 2006.
601 Hughen, K. A., T. I. Eglinton, L. Xu and M. Makou, Abrupt tropical vegetation response to rapid
602 climate changes, *Science, 304*, 1955-1959, 2004.
603 Jahn, B., Donner, B., Müller, P. J., Röhl, U., Schneider, R. R., and Wefer, G. Pleistocene variations in dust
604 input and marine productivity in the northern Benguela Current: evidence of evolution of
605 global glacial–interglacial cycles. *Palaeogeography, Palaeoclimatology, Palaeoecology*, 193,
606 515-533, 2003.
607 Jansen, J. H. F., A. Kuijpers and S. R. Troelstra, A Mid-Brunhes Climatic Event - Long-Term Changes in
608 Global Atmosphere and Ocean Circulation, *Science, 232*, 619-622, 1986.
609 Jouzel, J., Masson-Delmotte, V., Cattani, O., Dreyfus, G., Falourd, S., Hoffmann, G., and Wolff, E. W.
610 Orbital and millennial Antarctic climate variability over the past 800,000 years. *Science*,
611 317(5839), 793-796, 2007.

612 Jury, M. R., Valentine, H. R., and Lutjeharms, J. R. Influence of the Agulhas Current on summer rainfall
613 along the southeast coast of South Africa, *J. Appl. Meteorol.*, 32, 1282–1287, 1993.
614 Just, J., Schefuß, E., Kuhlmann, H., Stuut, J.B.W. and Pätzold, J., 2014. Climate induced sub-basin
615 source-area shifts of Zambezi River sediments over the past 17ka. *Palaeogeography,*
616 *Palaeoclimatology, Palaeoecology, 410*, 190-199.
617 Khon, V.C., Wang, Y.V., Krebs-Kanzow, U., Kaplan, J.O., Schneider, R.R. and Schneider, B., 2014.
618 Climate and CO_2 effects on the vegetation of southern tropical Africa over the last 37,000
619 years. *Earth and Planetary Science Letters, 403*, 407-417.
620 Lane, C.S., Chorn, B.T. and Johnson, T.C., 2013. Ash from the Toba supereruption in Lake Malawi
621 shows no volcanic winter in East Africa at 75 ka. *Proceedings of the National Academy of*
622 *Sciences, 110*, 8025-8029.
623 Lang, N., and Wolff, E. W. Interglacial and glacial variability from the last 800 ka in marine, ice and
624 terrestrial archives. *Climate of the Past*, 7(2), 361-380, 201.
625 Lisiecki, L. E. and M. E. Raymo, A Pliocene-Pleistocene stack of 57 globally distributed benthic delta
626 O-18 records, *Paleoceanography, 20*, 2005.
627 Lüthi, D., Le Floch, M., Bereiter, B., Blunier, T., Barnola, J. M., Siegenthaler, U., et al. High-resolution
628 carbon dioxide concentration record 650,000–800,000 years before present. Nature, 453,
629 379-382, 2008.
630 Martin, A.K. Evolution of the Agulhas Current and its palaeo-ecological implications. South African
631 Journal of Science, 77, 547-554, 1981.
632 Meckler, A., M. Clarkson, K. Cobb, H. Sodemann and J. Adkins, Interglacial Hydroclimate in the
633 Tropical West Pacific Through the Late Pleistocene, *Science, 336*, 1301-1304, 2012.

634 Past Interglacials Working Group of PAGES. Interglacials of the last 800,000 years. *Reviews of*
635 *Geophysics 54,* 162–219, 2016.
636 Peeters, F. J., Acheson, R., Brummer, G. J. A., De Ruijter, W. P., Schneider, R. R., Ganssen, G. M., Ufkes,
637 E., and Kroon, D. Vigorous exchange between the Indian and Atlantic oceans at the end of
638 the past five glacial periods. *Nature*, *430*, 661-665, 2004.
639 Ponton, C., West, A.J., Feakins, S.J. and Galy, V., 2014. Leaf wax biomarkers in transit record river
640 catchment composition. *Geophysical Research Letters, 41*, 6420-6427.
641 Poynter, J. G., P. Farrimond, N. Robinson and G. Eglinton, Aeolian-derived higher plant lipids in the
642 marine sedimentary record: links with palaeoclimate, in Paleoclimatology and
643 paleometeorology : modern and past patterns of global atmospheric transport, edited by M.
644 Leinen and M. Sarnthein, pp. 435-462, Kluwer, Dordrecht, 1989.
645 Reason, C. J. C. and Mulenga, H. Relationships between South African rainfall and SST anomalies in
646 the Southwest Indian Ocean, *Int. J. Climatol., 19*, 1651–1673, 1999.
647 Rommerskirchen, F., G. Eglinton, l. Dupont, U. Guntner, C. Wenzel and J. Rullkotter, A north to south
648 transect of Holocene southeast Atlantic continental margin sediments: Relationship between
649 aerosol transport and compound-specific $\delta^{13}C$ land plant biomarker and pollen records,
650 *Geochem. Geophy. Geosy., 4*, 2003.
651 Rommerskirchen, F., G. Eglinton, L. Dupont and J. Rullkoetter, Glacial/interglacial changes in southern
652 Africa: Compound-specific delta C-13 land plant biomarker and pollen records from
653 southeast Atlantic continental margin sediments, *Geochemistry Geophysics Geosystems, 7*,
654 2006.
655 Schefuß, E., Kuhlmann, H., Mollenhauer, G., Prange, M. and Pätzold, J., 2011. Forcing of wet phases in
656 southeast Africa over the past 17,000 years. *Nature, 480*, 509-512.

657 Schefuß, E., S. Schouten, J. H. F. Jansen and J. S. Sinninghe Damsté, African vegetation controlled by
658 tropical sea surface temperatures in the mid-Pleistocene period, *Nature, 422*, 418-421, 2003.
659 Scholz, C. A., T. C. Johnson, A. S. Cohen, J. W. King, J. A. Peck, J. T. Overpeck, M. R. Talbot, E. T. Brown,
660 L. Kalindekafe, P. Y. O. Amoako, R. P. Lyons, T. M. Shanahan, I. S. Castañeda, C. W. Heil, S. L.
661 Forman, L. R. McHargue, K. R. Beuning, J. Gomez and J. Pierson, East African megadroughts
662 between 135 and 75 thousand years ago and bearing on early-modern human origins,
663 *Proceedings of the National Academy of Sciences of the United States of America, 104*,
664 16416-16421, 2007.
665 Schulz, H., Lückge, A., Emeis, K.C. and Mackensen, A. Variability of Holocene to Late Pleistocene
666 Zambezi riverine sedimentation at the upper continental slope off Mozambique, 15–21 S.
667 *Marine Geology*, 286, 21-34, 2011.
668 Sinninghe Damsté, J. S., Verschuren, D., Ossebaar, J., Blokker, J., van Houten, R., van der Meer, M. T., ...
669 & Schouten, S. A 25,000-year record of climate-induced changes in lowland vegetation of
670 eastern equatorial Africa revealed by the stable carbon-isotopic composition of fossil plant
671 leaf waxes. *Earth and Planetary Science Letters, 302*, 236-246, 2011.
672 Tierney, J. E., Russell, J. M., & Huang, Y. A molecular perspective on Late Quaternary climate and
673 vegetation change in the Lake Tanganyika basin, East Africa. Quaternary Science *Reviews*, 29,
674 787-800, 2010.
675 Trauth, M.H., Larrasoaña, J.C. and Mudelsee, M., 2009. Trends, rhythms and events in Plio-Pleistocene
676 African climate. *Quaternary Science Reviews, 28*, 399-411.
677 Tyson, P. D. and Preston-Whyte, R. A.: The weather and climate of Southern Africa, Oxford University
678 Press, Cape Town, 2000.

van der Lubbe, H.J.L., Frank, M., Tjallingii, R. and Schneider, R.R. Neodymium isotope constraints on provenance, dispersal, and climate-driven supply of Zambezi sediments along the Mozambique Margin during the past~ 45,000 years. *Geochemistry, Geophysics, Geosystems, 17*, 181-198, 2016.

van der Lubbe, H.J.L., Tjallingii, R., Prins, M.A., Brummer, G.J.A., Jung, S.J., Kroon, D. and Schneider, R.R.. Sedimentation patterns off the Zambezi River over the last 20,000 years. *Marine Geology*, 355, 189-201, 2014.

Vogts, A., Moossen, H., Rommerskirchen, F., & Rullkötter, J. Distribution patterns and stable carbon isotopic composition of alkanes and alkan-1-ols from plant waxes of African rain forest and savanna C_3 species. *Organic Geochemistry*, *40*, 1037-1054, 2009.

Vogts, A., Schefuß, E., Badewien, T., & Rullkötter, J. *n*-Alkane parameters from a deep sea sediment transect off southwest Africa reflect continental vegetation and climate conditions. *Organic Geochemistry* 47, 109-119, 2012.

Weijer, W., De Ruijter, W. P., Sterl, A., & Drijfhout, S. S. (2002). Response of the Atlantic overturning circulation to South Atlantic sources of buoyancy. Global and Planetary Change, 34(3), 293-311.

Weijers, J. W. H., S. Schouten, J. C. van den Donker, E. C. Hopmans and J. S. Sinninghe Damsté, Environmental controls on bacterial tetraether membrane lipid distribution in soils, *Geochimica et Cosmochimica Acta, 71*(3), 703-713, 2007.

White, F. (1983). The vegetation of Africa. A descriptive memoir to accompany the UNESCO/AETFAT/UNSO vegetation map of Africa. *Natural Resources Research*, 20, UNESCO, Paris, 1983.

Yin, Q. Insolation-induced mid-Brunhes transition in Southern Ocean ventilation and deep-ocean temperature. *Nature*, 494(7436), 222-225, 2013.

Figure Captions

Figure 1: Map of the southern African continent with core locations and major surface currents drawn based on Caley et al. (2011). The locations of marine cores MD96-2048 (this study), MD96-2077 (Bard and Rickaby, 2009) and ODP Site 1082 (Jahn et al., 2003) are shown. The Zambezi and Limpopo River basins are outlined by the light and dark gray shading, respectively. The black line drawn on southern region of the continent indicates the location of the Great Escarpment. The location of Maputo (M) is given by the white dot and the approximate location of drill core MAL05-1c from Lake Malawi is indicated (Scholz et al., 2007; Cohen et al., 2011; Beuning et al., 2011). The Agulhas Current (AC), Agulhas Return Current (ARC), Benguela Current (BC) are the major surface currents in the region and are shown by the labelled arrows. Sites of retroflection and recirculation are noted. The approximate location of eddies of the Mozambique Channel (Moz.), East Madagascar Current, and the Agulhas Rings, which transport heat and salt into the Atlantic Ocean, are indicated. The dashed line indicates the location of the subtropical front (STF). B) The plant geographical regions of southern Africa (figure modified from Dupont et al. (2011), which is based on White, 1983). The five regions relevant for our study are Zambezian (tropical, mainly savanna and woodland), Zanzibar-Inhambane (tropical, mainly forest), Highveld (subtropical grassland), Tongaland-Pondoland (subtropical forest) and Afromontane (White, 1983).

Figure 2: MD96-2048 *n*-alkane data. a) The concentration of the nC_{27}, nC_{29}, nC_{31} and nC_{33} *n*-alkanes. The C_{31} *n*-alkane is the most abundant of the long-chain *n*-alkanes (mean concentration of 0.10 µg g sed^{-1}) followed by the C_{33} *n*-alkane (mean concentration of 0.09 µg g sed^{-1}) and the C_{29} *n*-alkane (mean concentration of 0.05 µg g sed^{-1}). b) The mass accumulation rate (MAR) of long-chain *n*-alkanes (sum of C_{27} to C_{33}; black circles) and c) the MAR of total branched glycerol dialkyl glycerol

tetraethers (GDGTs; open gray triangles). d) The average chain length (ACL). e) The carbon isotopic composition of the C_{31} *n*-alkane ($\delta^{13}C_{wax}$). f) The $C_{31}/(C_{29}+C_{31})$ *n*-alkane ratio. In D, E and F the horizontal lines plot the mean values for the 800-430 ka and 430-0 ka intervals. The vertical dashed line at 430 ka indicates the MBE. The Marine Isotope Stages (MIS) are indicated by the numbers at the top of panel E.

Figure 3: Summary of paleoclimate records during the past 800 ka. a) The carbon isotopic composition of the C_{31} *n*-alkane ($\delta^{13}C_{wax}$). The thick green line represents the smoothed data (5 point running mean). Higher (less negative) values indicate increased inputs from C_4 vegetation. b) Average chain length (ACL). Higher ACL values occur at times of lower SST and thus are likely mainly reflecting changes in aridity. c) The $C_{31}/(C_{29}+C_{31})$ *n*-alkane ratio. The y-axis is reversed. Higher values suggest increased inputs of grasses (C_{31}) and likely reflect arid conditions. d) The SST record of core MD96-2048 based on the stacked record of the $U^{K'}_{37}$ Index, Mg/Ca ratios of *G. ruber* s.s., and TEX_{86}. Data from Caley et al. (2011). In b, c, and d, the straight gray line indicates the overall trend over the past 800 ka. e) The global benthic oxygen isotope ($\delta^{18}O$) stack is shown for comparison (Lisiecki and Raymo, 2005). Marine Isotope Stages (MIS) are indicated by the gray boxes and numbers at the bottom and top of the graph. The vertical blue bars and roman numerals at the top indicate glacial terminations. With the exception of SST (d), all y-axes are reversed.

Figure 4: Comparison between *n*-alkane parameters and pollen assemblage data for the past 350 ka. All pollen data are from Dupont et al. (2011). In a, b and c the results of end-member modeling of the pollen assemblages are displayed (note the reversed y-axes). EM3 is plotted in a) and represents a complex assemblage of different biomes with woodland and forest taxa combined with coastal

750 vegetation. EM1 is plotted in b) and represents humid mountainous *Podocarpus* forest and
751 woodland taxa. EM2 is plotted in c) and represents open mountain vegetation dominated by
752 ericaeceous scrubs. d) The SST record of MD96-2048 from Caley et al. (2011). e) The carbon isotopic
753 composition of the C_{31} *n*-alkane ($\delta^{13}C_{wax}$). The black line is the 5 point running mean. f) The
754 $C_{31}/(C_{29}+C_{31})$ *n*-alkane ratio. g) The percent of woodland and forest pollen in core MD96-2048. It is
755 notable that woodland/forest pollen is present throughout the entire record. The Marine Isotope
756 Stages (MIS) are indicated by the gray boxes and numbers at the bottom and top of the graph. Note
757 the relationships between EM2, SST and the $C_{31}/(C_{29}+C_{31})$ *n*-alkane ratio, supporting that SW Indian
758 Ocean SST is a main control on the vegetation of southern East Africa.
759
760 **Figure 5:** Cross-spectral analysis between the SST stack (Caley et al., 2011) and the $C_{31}/(C_{29}+C_{31})$
761 ratio from site MD96-2048. a) power spectra (log-scale) showing the SST record in black and the
762 $C_{31}/(C_{29}+C_{31})$ ratio in gray, b) coherence with the 80 and 95% confidence intervals indicated by the
763 dashed lines, and c) phase in degrees. Strong 41 kyr cyles are noted in the SST and $C_{31}/(C_{29}+C_{31})$
764 ratio supporting the role of obliquity in driving SW Indian Ocean SST and vegetation change in
765 southern East Africa.
766
767 **Figure 6:** Box and whisker plots highlighting the differences between pre- and post-MBE intervals in
768 MD96-2048. In all plots the bottom and top of the box indicate the first and third quartiles while the
769 solid line inside the box indicates the median (the second quartile). The dashed line inside of the box
770 indicates the mean, which in a few cases plots on top of the median line. The tips of the whiskers
771 represent the smallest and largest values that are not more than 1.5 times the interquartile range
772 above or below the median. The dots represent the outliers. For all plots, a Student's t-test significant

773 at a 95% confidence level was first performed to test the null hypothesis that the means of the pre-
774 and post-MBE intervals are the same; for all parameters the null hypothesis was rejected. a) The
775 global benthic LR04 oxygen isotope stack (Lisiecki and Raymo, 2005). b) Carbon dioxide (CO_2) data
776 from the EPICA Dome C ice core (Luthi et al., 2008) in units of parts per million by volume (ppmv). c)
777 MD96-2048 *n*-alkane average chain length (ACL) values. d) MD96-2048 $C_{31}/(C_{29}+C_{31})$ *n*-alkane ratio.
778 e) SST stack at site MD96-2048. Data from Caley et al. (2011). The range of the data for the pre- and
779 post-MBE intervals is indicated on the plots.

Figure 1

Click here to download Figure: Figure 1 revised.pdf

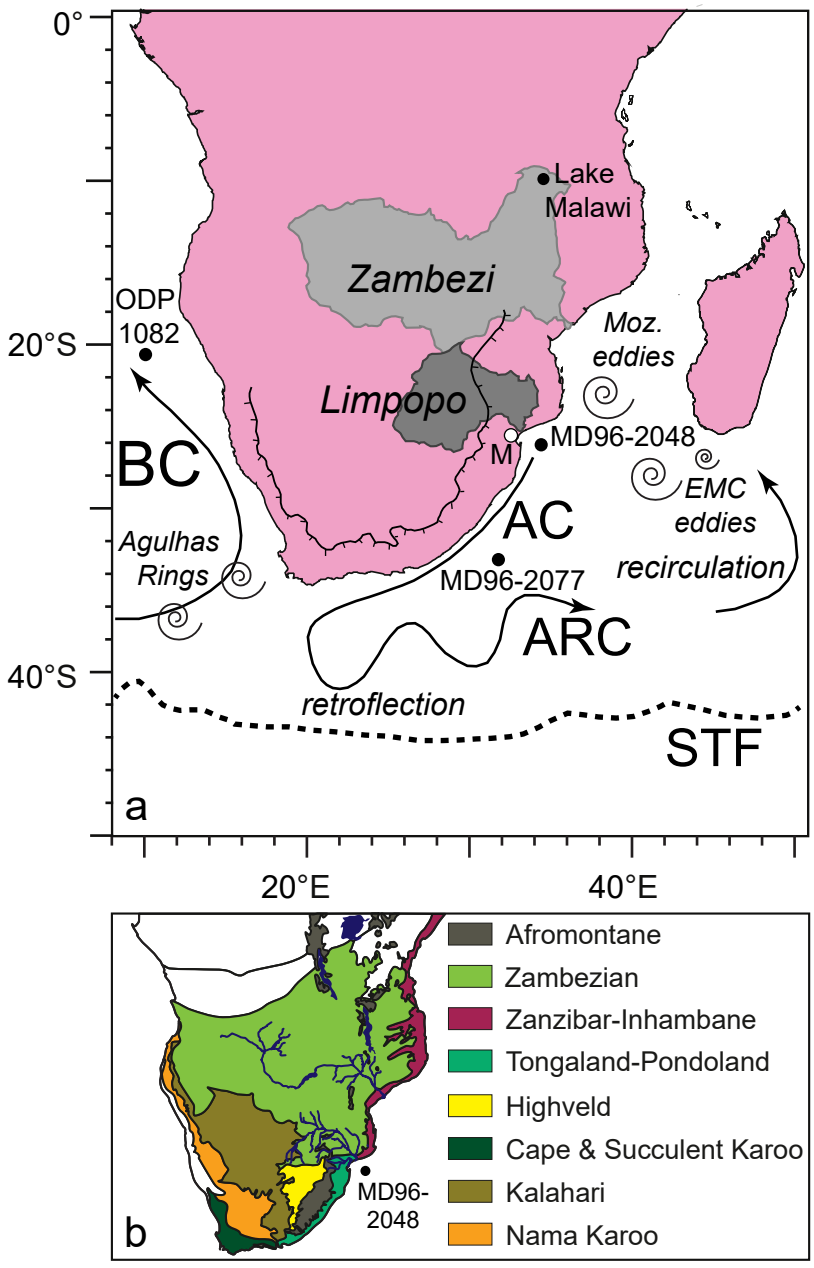

Figure 1

Figure 2

Click here to download Figure: Figure 2 revised.pdf

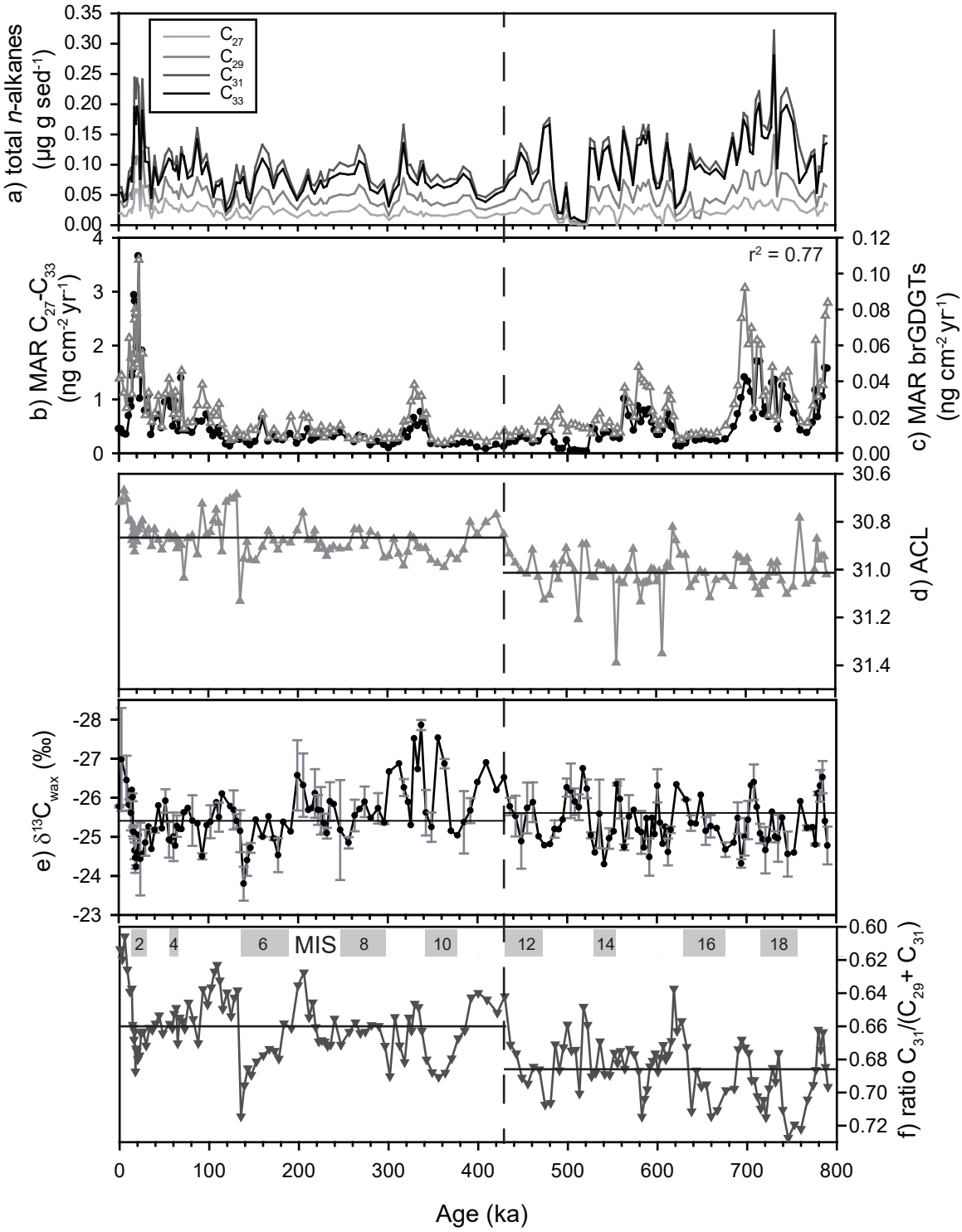

Figure 2

Figure 3

Click here to download Figure: Figure 3 revised.pdf

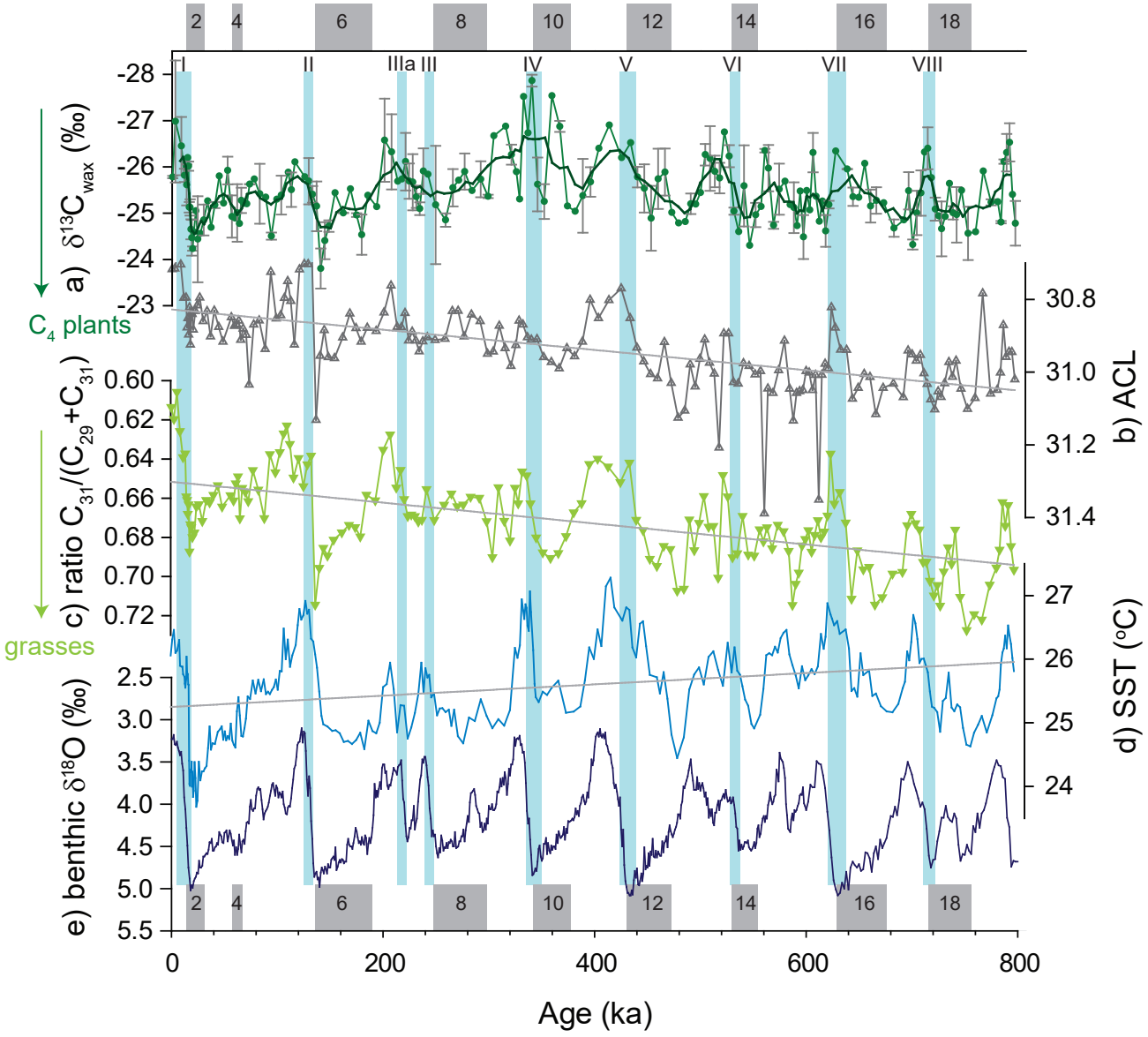

Figure 3

Figure 4

Click here to download Figure: Figure 4 revised.pdf

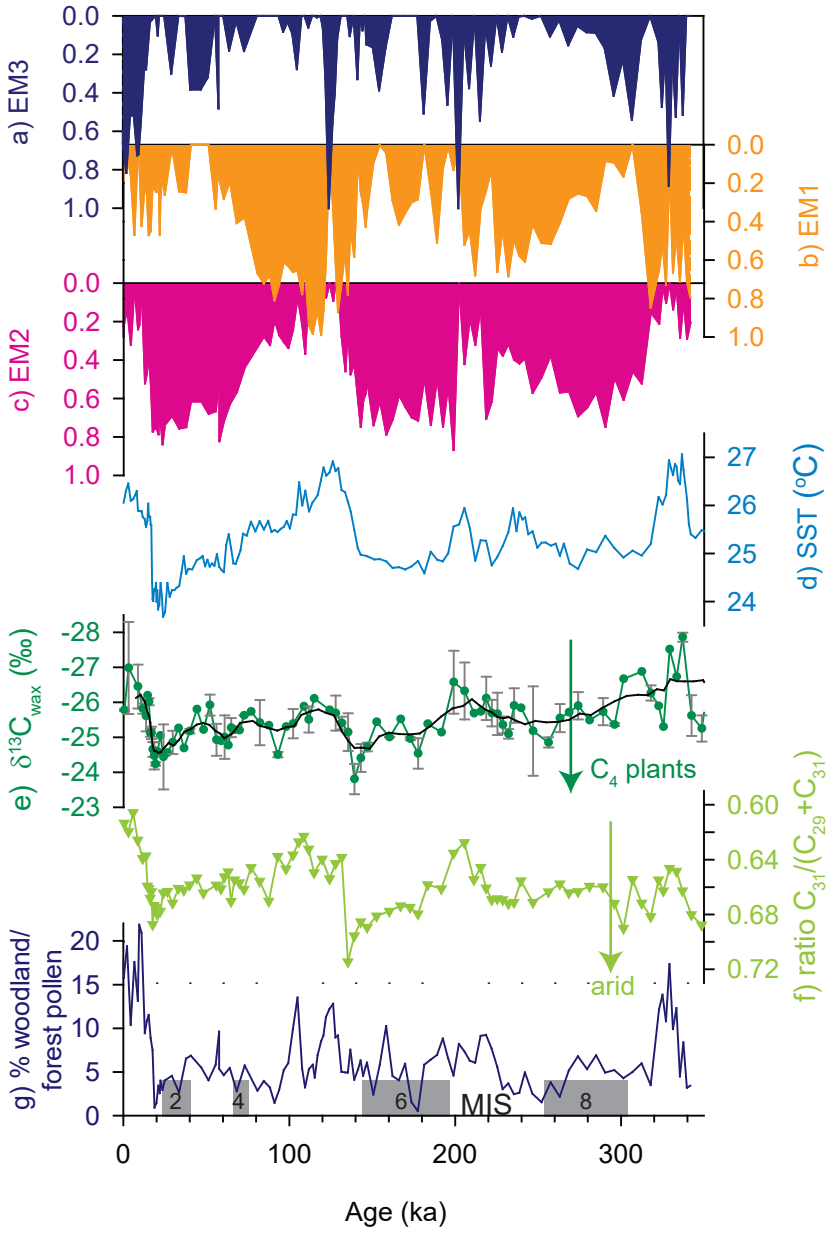

Figure 4

Figure 5

Click here to download Figure: Figure 5 revised.pdf

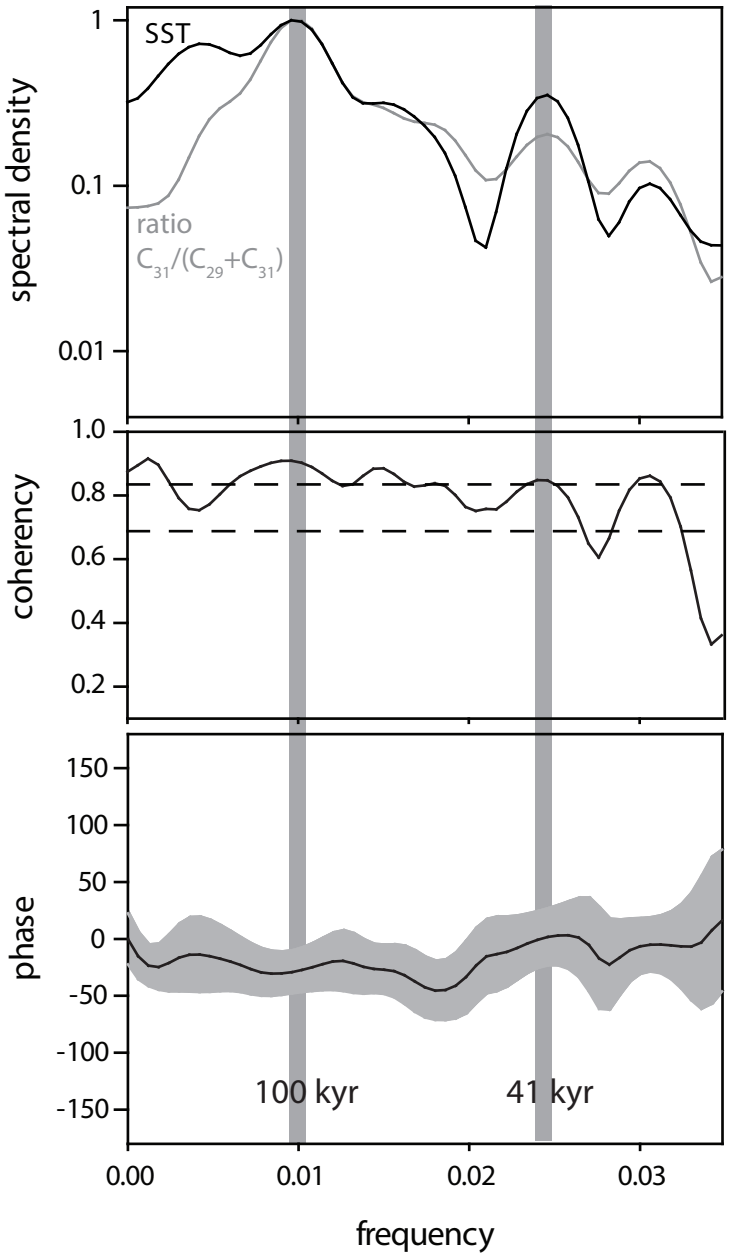

Figure 5

Figure 6

Click here to download Figure: Figure 6 revised.pdf

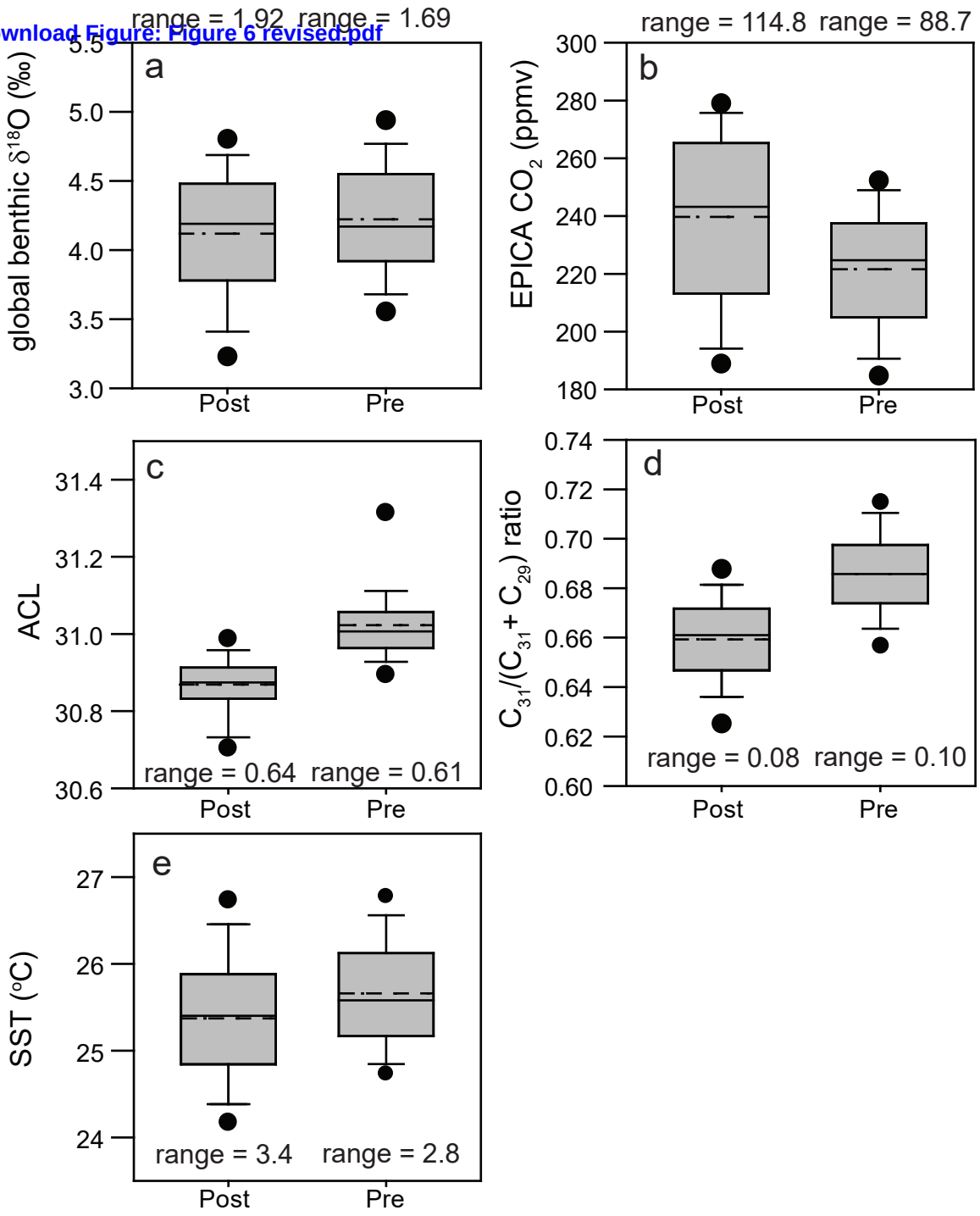

Figure 6